On the Delamination Self-Sensing Function of Z-pinned Composite Laminates

B. Zhang[a,*], G. Allegri[b], M. Yasaee[a], S.R. Hallett[a], I.K. Partridge[a]

[a]Advanced Composites Centre for Innovation and Science (ACCIS),

University of Bristol, Queen's Building, University Walk, Bristol BS8 1TR, UK

[b] Department of Aeronautics, Imperial College London,

South Kensington Campus, London SW7 2AZ, UK

Abstract

This paper investigates for the first time the usage of through-thickness reinforcement for delamination detection in self-sensing composite laminates. Electrically conductive T300/BMI Z-pins are considered in this study. The through-thickness electrical resistance is measured as the delamination self-sensing variable, both for conductive and non-conductive laminates. The Z-pin ends are connected to a resistance measurement circuit via electrodes arranged on the surface of the laminate. The delamination self-sensing function enabled by conductive Z-pins is characterised for Mode I/II delamination bridging, using single Z-pin coupons. Experiment results show that, if the through-thickness reinforced laminate is electrically conductive, the whole Z-pin pull-out process associated with delamination bridging can be monitored. However, for a non-conductive laminate, delamination bridging may not be sensed after the Z-pin is pulled out from one of the surface electrodes. Regardless of the electrical properties of the reinforced laminate, the through-thickness electrical resistance is capable of detecting Mode II bridging, albeit there exists an initial "blind spot" at relatively small lateral deformation. However, the Z-pin rupture can be clearly detected as an abrupt resistance increase. This study paves the way for exploring multi-functional applications of through-thickness reinforcement.

Keywords: A. Structural composites; A. Smart materials; B. Delamination; Z-pinning

*Corresponding author: b.zhang@bristol.ac.uk (B. Zhang); +44(0) 117 33 15311

1. Introduction

Multi-functional composites have attracted an increasing research interest over the past two decades. Multi-functionality usually involves a load-bearing capability coupled with strain/temperature/damage sensing, structural actuation and energy harvesting [1]. Multi-functional composites can be mainly classified into two: 1) additional-phase activated composites; 2) self-functioning composites. Typical examples of the former are carbon nanotube-filled composites, which offer both sensing and actuation functionalities [2,3]. On the other hand, a carbon-fibre reinforced polymer (CFRP) can be regarded as a self-functioning composite, as it offers an inherent delamination detection function through electrical resistance (ER) or electric potential measurements [4–6], without the need of embedding additional "smart" phases in the baseline material.

Traditional polymer-based composite laminates possess excellent in-plane performance, but they are prone to suffer delamination between plies, particularly when subjected to impact. Thus several through-thickness reinforcement (TTR) technologies such as stitching, 3D weaving and tufting have been developed to improve interlaminar strength and toughness of composite laminates [7]. Z-pinning is an effective TTR technology, whereby small diameter rods (Z-pins) are inserted through the thickness of laminates [8]. The mechanical performance of Z-pinned composites has been assessed in several experimental [9,10] and modelling studies [11–13]. However, regarding multi-functionality, only a single conceptual study on the sensing performance of TTR laminates comprising piezoelectric Z-pins is available in the literature [14].

The most commonly used Z-pins consist of small-scale (less than 1 mm diameter) CFRP rods, made of carbon-fibres consolidated into BMI matrix. In this study we consider 0.28 mm diameter Z-pins, which have 1k filament count tows and 63% theoretical fibre-volume-fraction. Small-scale CFRP rods can self-sense strain via

measurements of longitudinal ER [15]. This implies that, at least in principle, self-sensing functions may be enabled in TTR laminates by the presence of Z-pins.

This paper for the first time validates the usage of TTR for delamination detection in self-sensing composite laminates. The strain sensing capability provided by individual T300/BMI Z-pins under pure tension is considered first, via measurements of the longitudinal ER. Then, delamination sensing via through-thickness electrical resistance (TTER) measurements is investigated in carbon/epoxy (CFRP) and glass/epoxy (GFRP) single Z-pin coupons, under Mode I and Mode II regimes.

2. Specimen preparation

Fig. 1 shows the configuration of single Z-pin tension coupons, which had a 20 mm gauge length. Tensile loading was applied via two GFRP tabs, which were bonded to the pin using AS89.1/AW89.1 adhesive (Cristex Ltd, UK). The bonding length was 25 mm on each side. The tabs were aligned to the Z-pin using a paper card [16]. Two outer electrodes and two inner electrodes were bonded to the Z-pin ends, for current injection and voltage measurement respectively. Thus a 4-wire ER measurement set-up was employed in order to factor out the effect of Z-pin/electrode contact ER. Silver/epoxy conductive adhesives (1:1 weight ratio) were used for manufacturing the electrodes. These were cured at 80 °C for 15 minutes in an oven. The electrodes were positioned outside of the gauge length, in order to avoid damaging the Z-pin/electrode interfaces while applying loading. Each electrode was also bonded to a conductive wire.

As shown in Fig. 2a, the coupon configuration for single Z-pin bridging tests is analogous to that considered in [9], although some modifications were introduced in order to accommodate the electrodes. The coupon consists of a prismatic laminate block, which is split into two halves on the mid-plane by a PTFE release film. The laminate was made of 48 plies of unidirectional prepreg, with stacking sequence $[(-45/90/45/0)_s]_6$.

Two different prepreg materials were employed, namely: conductive carbon/epoxy IM7/8552; and non-conductive glass/epoxy E-glass/913 (Hexcel, UK). The average coupon thickness was 6.0 mm for CFRP and 6.8 mm for GFRP. A single Z-pin was inserted through the thickness of the laminate, with 1 mm long tips protruding from both the top and bottom surfaces of the laminate. Two prismatic electrodes were bonded to the protruding Z-pin ends. The electrodes were made of the same material employed for the tension coupons. Thus, a 2-wire ER measurement method was used in the bridging test. Each electrode had 5×5 mm^2 in-plane dimensions. For sake of clarity, a CFRP TTR rod connected to the electrodes is called a "sensing" Z-pin; otherwise, we shall refer to the TTR rod as a "mechanical" Z-pin.

Due to the electrode arrangement, the "sensing" Z-pin bridging coupon requires a different manufacture process in comparison with the "mechanical" Z-pin specimen described in [9]. More in detail, 1 mm thick rubber sheets were first placed on the bottom and top surfaces of the laminates. The Z-pins were inserted through the entire thickness of the laminate/rubber-sheet assembly, as shown in Fig. 2b. The Z-pin ends were then sheared off on the rubber sheets. The plate was then cured in an autoclave following the manufacturer's recommendations (2 hours at 180 °C with 100 psi pressure for CFRP, and 1 hour at 125 °C and 100 psi for GFRP). The rubber sheets were peeled off after cure, leaving 1 mm long Z-pin ends protruding on the laminate surfaces, as already mentioned above. Next, the plate was carefully cut into individual coupons, as shown in Fig. 2c. After the coupon surfaces were cleaned by acetone, the electrodes were positioned with the aid of removable moulds, as shown in Fig. 2d. Each mould had a central hollow slot to accommodate and shape the electrode, as well as a side slot to hold the wire in position. In the bridging coupon, the Z-pin ends were fully embedded within the electrodes.

3. Experimental set-up

All the tests were carried out via a calibrated Instron 8872 servo-hydraulic machine, equipped with a 1 kN load cell. For the tensile tests, the coupons were gripped at the end tabs, as shown in Fig. 3. The tensile load was applied at the rate of 0.1 mm/min. The paper card attached to the specimen for alignment was carefully cut into two halves along its central line prior to testing, as indicated in Fig. 3. As shown in Fig. 4a, Mode I loading was applied to the bridging coupons via two steel tabs. Two spacers were inserted between the specimen and each of the tabs, in order to protect the electrodes that embed the Z-pin ends. The spacers must be electrically insulating and high-stiffness, in order to eliminate any spurious effect on the TTER and reduce the overall loading-system compliance, respectively. In this study, each spacer consisted of a 20 × 4 × 3 mm^3 (length × width × thickness) E-glass/913 laminate block. The spacers were bonded to the coupon and the tabs using cyanoacrylate superglue (Loctite Corp., UK). As shown in Fig. 4b, Mode II loading was applied to the bridging specimens via a modified Arcan rig, as in [9]. The central plate of the rig can be rotated to obtain various mode mixities, albeit only a 90° orientation (Mode II) was used in this study. The plate comprises a central slot to accommodate the specimen. The testing coupon was attached to the top and bottom halves of the plate using two screw clamps. These also allowed inserting electrically insulating PVC tape between the coupon and the jig. As shown in Fig. 4c, each half of the plate also comprised a radially oriented slot, which was designed to contain the electrodes and the wires connecting the specimen to the signal acquisition system. The Mode I and Mode II loads were both applied at a displacement rate of 0.5 mm/min. The ER signal was measured by a Keithley 2700 digital multimeter with resolution and sample rate of 6.5 digits and 20 readings/s, respectively.

4. Results and discussions

4.1 Tension tests

Figs. 5a-b present the results of three tension specimens. All the coupons showed a consistent mechanical response. The stress increases linearly with the tensile strain until catastrophic Z-pin failure; all the Z-pins failed in the gauge region. The failure strength and strain are 2021 MPa and 1.5%, respectively. ASTM D3039 tests on unidirectional T300-12k carbon epoxy give a tensile strength of 1860 MPa [12]. The stressed volume for ASTM D3039 coupons is 2250 mm^3, while it is only 1.23 mm^3 for the tensile specimens considered here. Assuming a Weibull modulus of 27 [12], Weibull's strength theory suggests a failure stress of 2456 MPa for 0.28 mm Z-pins. The former value is 20% higher than that obtained experimentally, but this is reasonable considering the difference of filament count and resin system with respect to the material characterised in [12]. The strength value obtained here also agrees well with that recently reported in [17] for 0.28 mm T300/BMI Z-pins. However, Cartié et al. [10] reported a strength value in the region of 1200 MPa for 0.51 mm T300/BMI Z-pins. The difference is likely to be due to a poorer consolidation of the larger diameter of T300/BMI Z-pins. Extensive porosity was observed in 0.51 mm diameter Z-pins, while 0.28 mm appeared properly impregnated [18]. Overall, the considerations drawn above support the validity of the tension test results presented here.

Fig. 5b shows the sensing behaviour of the Z-pin subjected to tensile loading. The initial ER values (R_0) of the three coupons are 76.1 Ω, 67.0 Ω and 83.3 Ω respectively. All the coupons also present a consistent ER trend. The ER first increases linearly up to around 0.8% strain (labelled by a plus sign in Fig. 5b), due to the elastic deformation of the Z-pin. With further loading, the ER increases at a higher rate until complete pin failure. This can be attributed to progressive random fibre breakage within the Z-pin

[15], whose onset takes place at 50% of the macroscopic failure load. The ER gauge factors for the tested coupons have consistent values up to 0.8% strain, for which $\Delta R/R_0$ = 0.035. On the other hand, above 0.8% strain, the gauge factor shows a significant variation from coupon to coupon. In order to explain this variation, it must be considered that the contacts between adjacent fibres are randomly distributed throughout the whole gauge region. This randomness is further promoted when fibre failure occurs, i.e. in the strain range where the gauge factors become nonlinear.

4.2 Bridging tests

Eight bridging coupons were tested for each laminate material, namely CFRP and GFRP. Four of the coupons were characterised under Mode I loading, while the remaining were tested in Mode II.

4.2.1 Z-pin reinforced CFRP laminates

The typical Mode I response for a single sensing Z-pin reinforced CFRP laminate is shown in Fig. 6a. For comparison, Fig. 6a also shows the bridging force provided by a mechanical Z-pin when pulled out from a laminate. The latter was made of the same material and had identical stacking sequence to the sensing Z-pin coupon considered here. The overall pull-out process for the sensing Z-pin comprises three stages: pre-debonding from electrode (stage I), pull-out from electrode (stage II) and pull-out from laminate (stage III). For sake of clarity, we will consider debonding and pull-out always starting from and initially progressing within the “top” electrode. During stage I, the bridging force increases linearly with the pin elastic elongation, as shown in the zoomed view in Fig. 6b. Due to the quasi-isotropic stacking sequence of the coupon, the Z-pin/laminate interface is severely weakened after the post-cure cool down [9,13]. This is also confirmed by observing the mechanical Z-pin pull-out force in Fig. 6a, whereby no load drop corresponding to Z-pin/laminate debonding appears. Thus, the sensing Z-

pin bridging force during stage I is mainly due to the Z-pin/electrode bonding and the Z-pin/laminate friction. The load peak that occurs at a small opening displacement corresponds to the onset of debonding from the top electrode. This dis-bond suddenly develops and the consequent load drop is also accompanied by a shortening of the Z-pin. Regarding the TTER during stage I, part of the injected current flows from the top to the bottom electrode, crossing the Z-pin/electrode interfaces and travelling along the Z-pin, as illustrated by a red dashed line in Fig. 7a. Since the CFRP laminate is conductive, part of the current also flows through the laminate thickness, crossing the Z-pin/laminate interfaces and eventually reconnecting with the Z-pin, as shown by red solid lines in Fig. 7a. The total TTER associated with the top half of the coupon, R_T, can be estimated as:

$$R_T \sim (R_{TEd_Pin} + R_{TPin}) \,//\, (R_{TEd_TLm} + R_{TLm} + R_{TLm_Pin}) \quad (1)$$

where "//" denotes the "resistors in parallel" operator; R_{TEd_Pin} is the contact ER between the top electrode and the Z-pin; R_{TPin} is the longitudinal ER of the top half Z-pin, whose value can be estimated from the tension test results and the exerted bridging force; R_{TEd_TLm} is the contact ER between the top electrode and the top sub-laminate, which is assumed constant with loading. Finally, R_{TLm} is the ER associated with the current path in the top sub-laminate, while R_{TLm_Pin} is the contact ER between the top sub-laminate and the Z-pin. Thus, in Eq. (1), the two terms on the left side of the "//" symbol give the equivalent ER associated with the current path marked by the dashed line on the top half coupon in Fig. 7a. The terms on the right side represent the equivalent ER of the other (continuous lines in Fig. 7a) current path. The bottom half of the coupon can be represented by an equivalent ER network identical to the top half, thus the TTER trend can be determined based on the latter.

The TTER in stage I increases until the peak load is researched and suddenly drops

with the Z-pin/electrode debonding. The mechanisms causing the TTER to increase are: 1) the Z-pin elongation, increasing the R_{TPin} term in Eq. (1); 2) the reduction of the Z-pin/electrode contact area, caused by the cross-sectional contraction of the Z-pin due to the Poisson effect and the progressive failure of the Z-pin/electrode interface – all these mechanisms increase R_{TEd_Pin}; (3) the reduction of the Z-pin/laminate contact area, which is also a result of the cross-sectional pin contraction and that raises R_{TLm_Pin}. For the same reason, the TTER decrease is due to the reduction of R_{TPin} induced by the Z-pin shortening, as well as the decrease of R_{TEd_Pin} and R_{TLm_Pin} due to the radial pin expansion induced by the Poisson effect. The comparison between Fig. 6b and Fig. 5b reveals that the fractional TTER increase during stage I pull-out is 40 times larger than in a tension coupon. This is because the TTER change is a consequence of the three aforementioned effects, while only the first mechanism, i.e. the Z-pin elongation, is responsible for the ER variation in the tension coupon.

In stage II, the Z-pin starts to slide within the top electrode and the top sub-laminate, as illustrated in Fig. 7b. The bridging force shows a stable increasing trend, as shown in Fig. 6b. This is due to two enhanced friction regions (EFRs), i.e. those due to snubbing [11], located at the ends of the Z-pin/top-laminate interface, as indicated in Fig. 7b. The EFR located near the fracture surface is caused by Z-pin misalignment [9,13]. The EFR close to top electrode is due to the dragging of the protruding Z-pin end into the laminate. Part of electrode material is squeezed in between the Z-pin and the laminate, locally increasing the friction. This will be confirmed in the next subsection. Further increasing the traction, the Z-pin tends to stay bonded to the bottom electrode. The traction reaches its peak when full pull-out from the top electrode is achieved, as for the coupon considered in Fig. 6. On the other hand, if the friction enhancement in the top sub-laminate is large enough, the Z-pin may also de-bond from the bottom electrode.

The second debonding is marked by another load drop, as observed in the coupon whose response is shown in Fig. 8. For this case, with further loading the Z-pin is gradually pulled out from the bottom electrode, with its top end stuck within the top electrode, as illustrated in Fig. 7c. The bridging force still exhibits an increasing trend, due to the two EFRs associated with the bottom half of the Z-pin. The traction reaches a second peak at the point where the Z-pin is fully pulled out from the bottom electrode. The different bridging mechanisms occurring in stage II are ultimately attributed to the coupon asymmetry relative to the fracture surface. The current paths in stage II are the same as in stage I, but the TTER signal during stage II becomes nosier due to the unstable Z-pin/electrode and Z-pin/laminate contact ERs. However, the overall TTER trend follows that of the load. In the case where debonding takes place only in one electrode, the TTER tends to increase during the whole stage II, as shown in Fig. 6b. This is simply because the Z-pin/electrode interface area decreases with progressive pull-out, and this raises the R_{TEd_Pin} term in Eq. (1). If debonding occurs in both electrodes, the TTER increases when the Z-pin slides within the top electrode. Then there is an ER drop corresponding to the second debonding, followed by a second ER increase due to sliding within the bottom electrode, as shown in Fig. 8. The TTER variation trend associated with the debonding from the bottom electrode can be explained using the same mechanisms identified for the debonding from the top electrode.

Stage III begins when the Z-pin is completely pulled out from one of the electrodes. The bridging force steadily decreases until complete pull-out from one of the sub-laminates, as shown in Fig. 6a and Fig. 8. The current path for stage III differs from those characterising stages I and II and it is illustrated in Fig. 7d and Fig. 7e, respectively for pull-out from the top sub-laminate (POFTL) and pull-out from the

bottom sub-laminate (POFBL). The difference arises because the current path associated with the $(R_{TEd_Pin} + R_{TPin})$ term in Eq. (1) disappears. Hence, for the POFTL case, the R_T value can be estimated as:

$$R_T \sim R_{TEd_TLm} + R_{TLm} + R_{TLm_Pin} \quad (2)$$

The onset of stage III is always marked by an abrupt TTER increase. This can be easily understood by comparing Eq. (1) and Eq. (2) and noticing that one of parallel resistors suddenly disappears. With further sliding, the current has to travel a longer distance through the laminate thickness before being able to reconnect with the Z-pin. This increases the R_{TLm} and R_{TLm_Pin} terms in Eq. (2), thus the TTER shows an overall increasing trend. However, the TTER is affected by noise, due to the variability in the Z-pin/laminate contact ER, which is further promoted by the progressive sliding. The above analysis also applies to the POFBL case.

As shown in Fig. 9, akin to a "mechanical" Z-pin [9], the Mode II bridging force provided by a sensing Z-pin also increases monotonically with the Z-pin deformation, until a catastrophic pin rupture occurs at relatively small sliding displacements. Regarding the TTER sensing, the current path in Mode II is the same as in stage I of Mode I. The Mode II TTER signal shows no clear trend for sliding displacements less than half the Z-pin diameter. Two opposite mechanisms are responsible for this behaviour. First, the Z-pin experiences an increasing lateral pressure due to the shear deformation. This will increase the effective Z-pin/electrode contact area through closing some of the voids existing at the interface, thus increasing the conductivity between the Z-pin tips and the electrodes, i.e. decreasing of the R_{TEd_Pin} term in Eq. (1). Moreover, the increasing lateral pressure will also raise the conductivity between adjacent Z-pin fibres due to current percolation, thus decreasing the R_{TPin} term in Eq. (1). Hence the lateral pressure in Mode II decreases the TTER. Conversely, the deformation

induces an axial stretching of the Z-pin, which increases the R_{TPin} term in Eq. (1). When the deformation exceeds half the Z-pin diameter, the TTER exhibits a steadily increasing trend. This is due to the progressive fibre failure that takes place within Z-pin segment close to the fracture plane [9,12,13]. The TTER becomes very large when the Z-pin has fully failed. Hence, the gauge factor shown in Fig. 9 appears to diverge.

4.2.2 Z-pin reinforced GFRP laminates

The CFRP Z-pin provides the same delamination bridging mechanism when inserted either in GFRP or CFRP laminates. This is true for both Mode I and Mode II loading. However, only the current paths indicated by red dashed lines in Fig. 7 exist in GFRP coupons, since the GFRP laminate is non-conductive. Thus, the R_T of the GFRP coupon in stages I and II can be estimated as:

$$R_T \sim R_{TEd_Pin} + R_{TPin} \tag{3}$$

For Mode I, as shown in Fig. 10b and Fig. 10d, the TTER provides a delamination sensing ability in stage I pull-out from a non-conductive laminate. The initial delamination opening can be sensed as a linear TTER increase, and the Z-pin/top-electrode debonding can be detected by an apparent TTER drop. The TTER becomes larger because R_{TPin} increases due to the Z-pin elongation, together with the raise of R_{TEd_Pin} due to the reduction of the Z-pin/electrode contact area. It is worth observing that the fractional TTER increase at stage I in the GFRP coupons is one order of magnitude less than in CFRP, because one of current paths is missing in the former.

In stage II, the TTER shows no clear overall changing trend. This is attributed to two opposite mechanisms: 1) the Z-pin/electrode contact ER, i.e. R_{TEd_Pin} in Eq. (3), becomes larger with the decrease in the Z-pin/electrode contact area; 2) the Z-pin misalignment promotes a local increase of contact forces at the EFR, which reduces R_{TEd_Pin}. The Z-pin/electrode debonding can be clearly detected as an abrupt ER

decrease in the GFRP coupon. The full pull-out from one of the electrodes can be detected by a further ER jump. In stage III, the current paths illustrated by red dashed lines in Figs. 7d-e may be interrupted in the sub-laminate where pull-out is taking place. Hence, the TTER may become extremely large and this implies losing sensing ability, as shown in Fig. 10a. However, quite surprisingly, the TTER signal presented in Fig. 10c reveals a sensing ability also for stage III. The reason for this rather peculiar behaviour can be understood via observing the post-mortem micrograph presented in Fig. 11. There is notable presence of carbon fibres, initially belonging to the Z-pin, which remained attached to the surface of the pull-out channel. These fibres provide electrical connection between the Z-pin and the electrode even when the pin end is dragged into the non-conductive laminate. In the enlarged view of Fig. 11, one can also observe debris of the electrode material being dragged into the pull-out channel. Apart from enhancing the Z-pin/laminate friction, these debris also contributes to maintain electrical connection during pull-out. However, the resulting TTER variation is characterised by a noise level much larger than in the CFRP coupons. Finally, as shown in Fig. 12, the Mode II response of a Z-pin in a non-conductive laminate can also be monitored via ER measurement. The TTER gauge factors for the Mode II response in GFRP laminates are similar to those observed in CFRP coupons. However, the "blind region" where no significant variation in ER occurs is larger in GFRP coupons than in CFRP laminates. An increase in TTER is noticeable only for lateral displacements exceeding one Z-pin diameter.

4.3 Discussion

A CFRP Z-pin is multi-functional, since it provides both a mechanical function (bridging) and a delamination sensing ability when inserted into composite laminates. A single CFRP Z-pin can be used to measure small tensile strains up to 0.8%,

corresponding to a longitudinal ER variation of 4%. Beyond the aforementioned threshold, it is impossible to obtain realistic strain values. Nonetheless, incipient damage (fibre failure) within the Z-pin can still be detected from the onset of non-linearity in the ER signal. When inserted in a laminate, the intrinsic Z-pin ER playes only a minor role in governing the TTER variation. The Z-pin/electrode contact ER, the Z-pin/laminate contact ER and the laminate conductivity (if any) all affect the resulting TTER. Eqs. (1)-(3) have introduced to help with the qualitative analysis of the various complementary and competing mechanisms involved in determining the TTER. An in-depth quantitative study is currently in progress and it will be reported in a separate paper. The main challenge to be faced is how to reliably predict contact resistances and this requires multi-physics micro-scale models. The experimental results presented in the Sec. 4.1-4.2 show that the intrinsic Z-pin ER variation represents less than 2% of the overall stage-I TTER-change under Mode I loading. The presence of contact ERs provide an amplification of the Z-pin effects on the resulting TTER, increasing the sensitivity to the presence of delamination, especially in comparison with the TTER sensing in an un-pinned laminate [19]. For load values below the initiation threshold of Z-pin/electrode debonding, the Z-pin ER may actually dominate the TTER, but this provide only a relatively narrow delamination sensing window.

In comparison with purely “mechanical” TTR, a sensing Z-pin is subjected to additional frictional forces provided by the Z-pin/electrode interface and the EFR formed due to the dragging of the protruding pin ends into the laminate. As such, the sensing Z-pin can provide a larger pull-out resistance, as demonstrated by Fig. 6a. Referring to the parametric study of Z-pin bridging ability in [13], the pin bridging performance in Mode I dominated cases may be improved due to the presence of the electrodes. However, when approaching a Mode II dominated regime, the sensing pin

may fail at a lower lateral deformation. Overall, the presence of electrodes may induce an earlier transition from complete pull-out to Z-pin failure with respect to the mode-mixity, albeit these effects need to be characterised with further tests and modelling.

5. Conclusions

This paper has investigated the self-sensing function of T300/BMI Z-pin reinforced composite laminates. Experimental results show that a CFRP Z-pin can perform as a strain sensor, having a gauge factor that is almost constant up to 0.8% elongation and that gradually increases under further deformation until complete failure. A simple 2-wire TTER measurement method was implemented for Z-pinned laminates. Two electrodes were attached to the Z-pin ends protruding from top and bottom surfaces of the laminate. The TTER variation allows monitoring the whole Mode I delamination bridging process in an electrically conductive laminate. The bridging mechanisms that can be sensed include: 1) the initial delamination loading detected as a linear ER increase; 2) the Z-pin/electrode debonding, sensed as an abrupt ER drop; 3) the Z-pin pull-out from the de-bonded electrode, detected as an overall ER increase; 4) the complete pull-out from one of the electrodes, corresponding to a sudden ER jump; 5) final pull-out stage from the laminate, characterised by an ER increase. On the other hand, if the laminate is non-conductive, the TTER allows sensing the progressive development of mechanisms 1, 2 and 4. Mechanism 3 cannot be sensed in non-conductive laminates. Mechanism 5 could also be sensed in non-conductive laminates, depending on the density of the residual Z-pin fibres that remain attached to the surface of the pull-out channel. The Mode II TTER exhibits a consistent increasing trend for both the conductive and non-conductive laminates, albeit there exists an initial “blind region” for relatively small lateral deformation in the order of one Z-pin diameter or less. However, the Z-pin rupture can be clearly detected as an abrupt TTER increase.

The electromechanical characterisation of Z-pins and reinforced laminates presented in this study provides the fundamentals for the development of multi-functional through-thickness reinforced composite structures.

Acknowledgements

The authors would like to acknowledge Rolls-Royce plc for the support of this research through the Composites University Technology Centre (UTC) at the University of Bristol.

References

[1] Pinto F. Smart multifunctional composite materials for improvement of structural and non-structural properties. PhD Dissertation, University of Bath, 2013.
[2] Gallo GJ, Thostenson ET. Electrical characterization and modeling of carbon nanotube and carbon fiber self-sensing composites for enhanced sensing of microcracks. Mater Today Commun 2015;3:17–26.
[3] Li C, Thostenson ET, Chou T-W. Sensors and actuators based on carbon nanotubes and their composites: A review. Compos Sci Technol 2008;68:1227–49.
[4] Wang X, Chung DDL. Continuous carbon fibre epoxy-matrix composite as a sensor of its own strain. Smart Mater Struct 1996;5:796–800.
[5] Todoroki A, Samejima Y, Hirano Y, Matsuzaki R. Piezoresistivity of unidirectional carbon/epoxy composites for multiaxial loading. Compos Sci Technol 2009;69:1841–6.
[6] Wang S, Chung DDL, Chung JH. Impact damage of carbon fiber polymer–matrix composites, studied by electrical resistance measurement. Compos Part A Appl Sci Manuf 2005;36:1707–15.
[7] Mouritz AP. Review of z-pinned composite laminates. Compos Part A Appl Sci Manuf 2007;38:2383–97.
[8] Partridge IK, Cartié DDR. Delamination resistant laminates by Z-Fiber® pinning: Part I manufacture and fracture performance. Compos Part A Appl Sci Manuf 2005;36:55–64.
[9] Yasaee M, Lander JK, Allegri G, Hallett SR. Experimental characterisation of mixed mode traction–displacement relationships for a single carbon composite Z-pin. Compos Sci Technol 2014;94:123–31.
[10] Cartié DDR, Cox BN, Fleck NA. Mechanisms of crack bridging by composite and metallic rods. Compos Part A Appl Sci Manuf 2004;35:1325–36.
[11] Cox BN. Snubbing effects in the pullout of a fibrous rod from a laminate. Mech Adv Mater Struct 2005;12:85–98.
[12] Allegri G, Yasaee M, Partridge IK, Hallett SR. A novel model of delamination bridging via Z-pins in composite laminates. Int J Solids Struct 2014;51:3314–32.
[13] Zhang B, Allegri G, Yasaee M, Hallett SR. Micro-mechanical finite element analysis of Z-pins under mixed-mode loading. Compos Part A 2015;78:424–35.
[14] Gu B, Zhang H, Wang B, Zhang S, Feng X. Fracture toughness of laminates reinforced by piezoelectric z-pins. Theor Appl Fract Mech 2015;77:35–40.

[15] Okuhara Y, Matsubara H. Memorizing maximum strain in carbon-fiber-reinforced plastic composites by measuring electrical resistance under pre-tensile stress. Compos Sci Technol 2005;65:2148–55.
[16] ASTM-C1557-03. Standard Test Method for Tensile Strength and Young's Modulus of Fibers. ASTM Int 2012.
[17] Wang X, Li C. Experimental study on pull-out strength of Z-pins. J Mater Eng 2011;1:1–4.
[18] Chang P, Mouritz AP, Cox BN. Properties and failure mechanisms of z-pinned laminates in monotonic and cyclic tension. Compos Part A Appl Sci Manuf 2006;37:1501–13.
[19] Shen L, Li J, Liaw BM, Delale F, Chung JH. Modeling and analysis of the electrical resistance measurement of carbon fiber polymer–matrix composites. Compos Sci Technol 2007;67:2513–20.

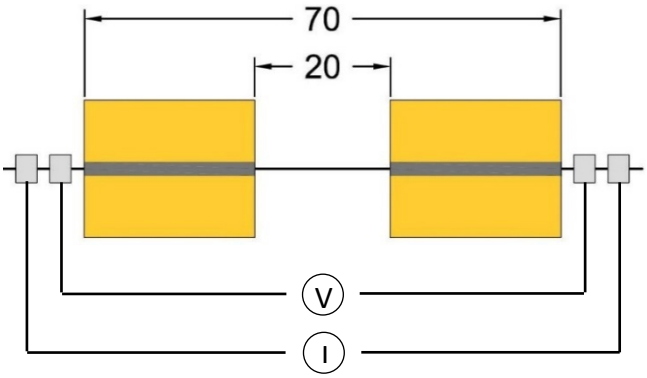


Fig. 1. Configuration of single Z-pin tensile test coupon (mm).

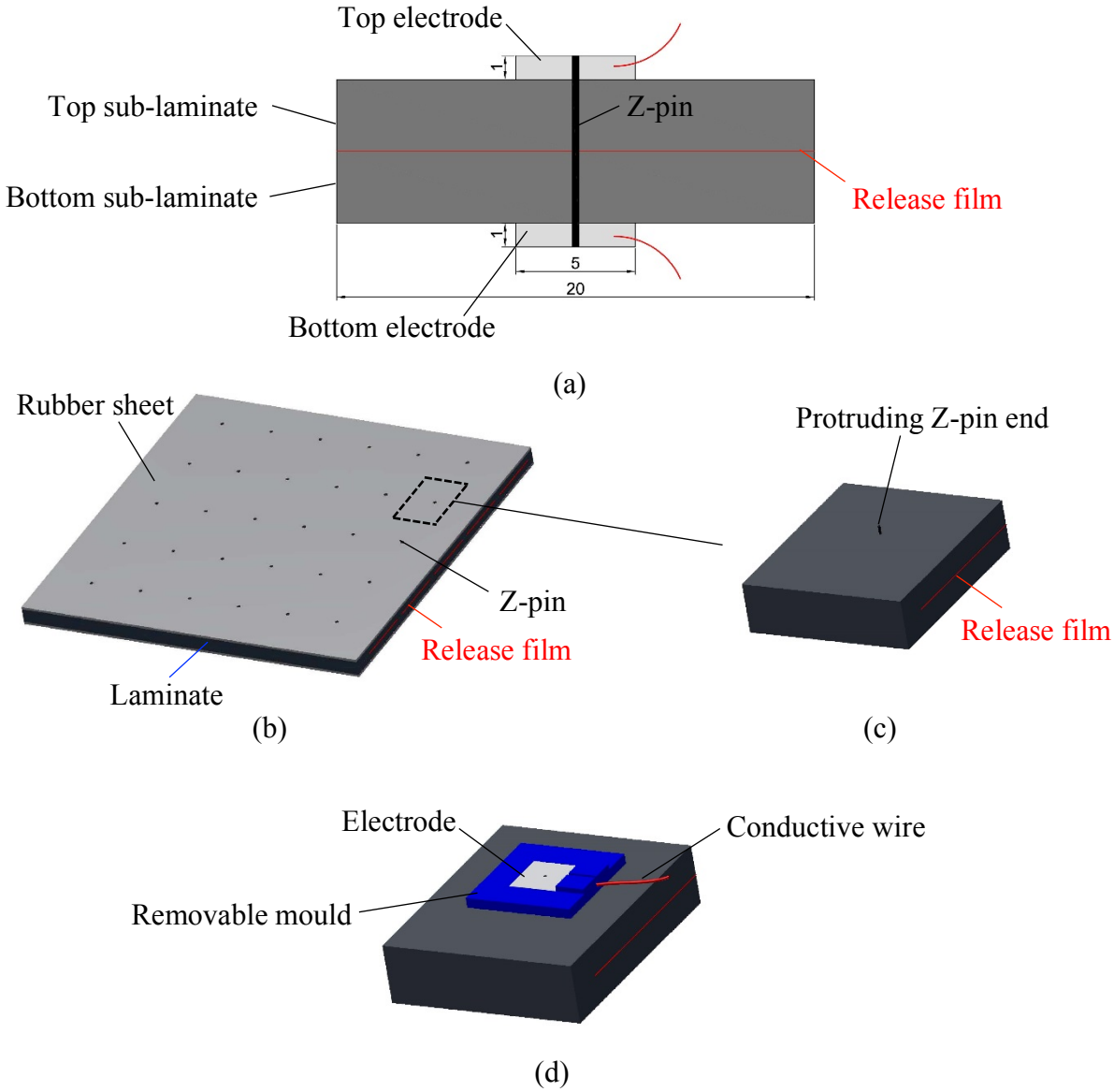


Fig. 2. (a) Single sensing Z-pin coupon for bridging test; (b) un-cured laminate plate with inserted pins and attached rubber sheets; (c) initial coupon with bare Z-pin ends; (d) electrode arrangement with the aid of removable moulds.

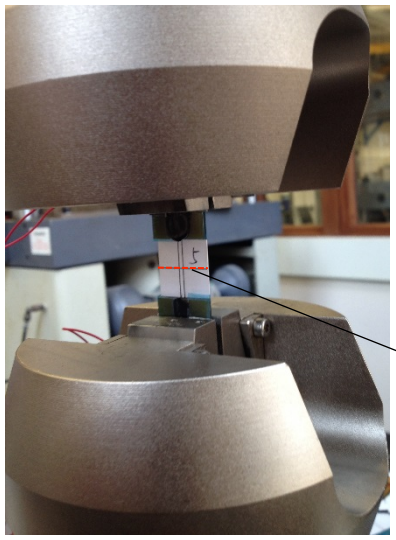
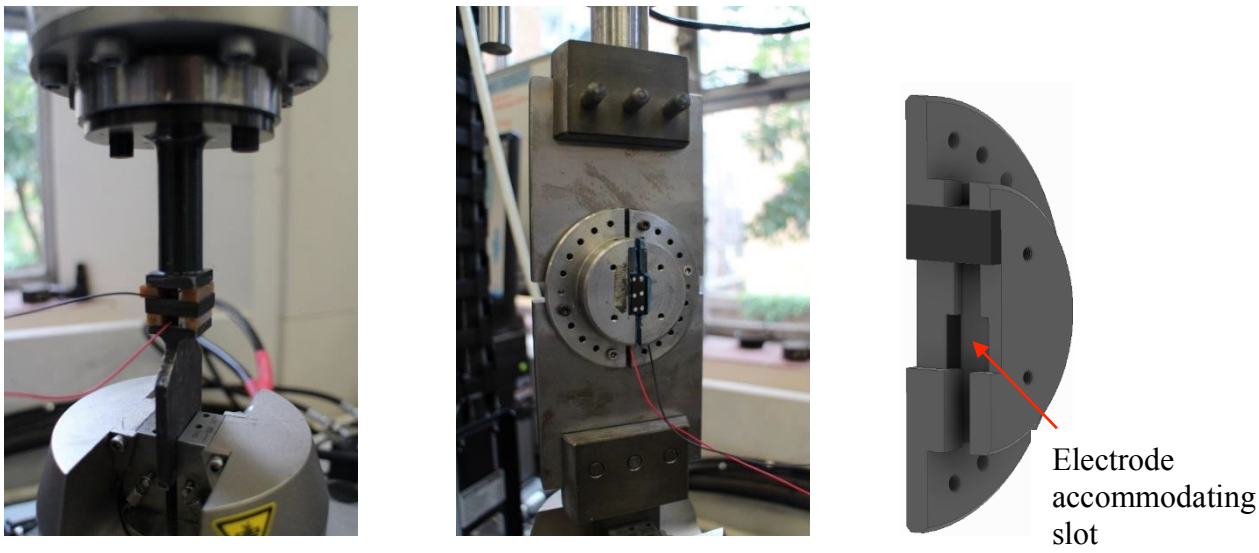
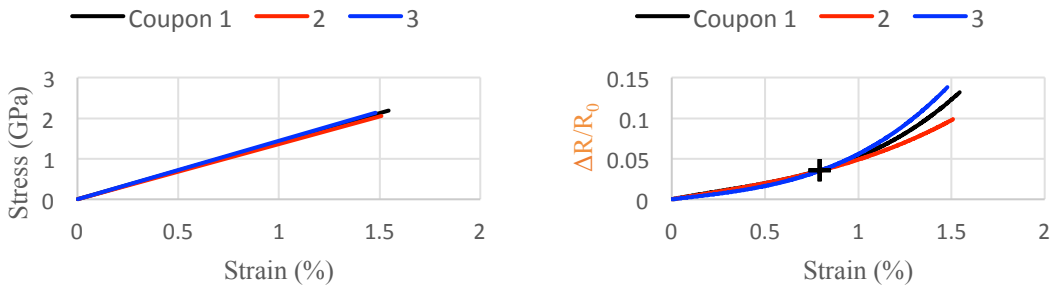


Fig. 3. Set-up for tensile loading.



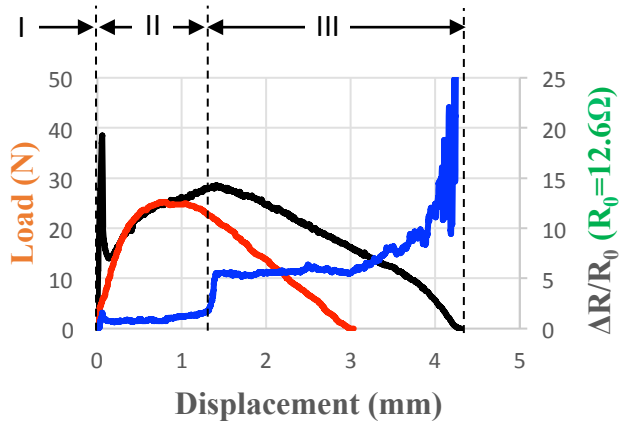
(a) (b) (c)

Fig. 4. Set-up for (a) Mode I and (b) Mode II bridging loading; (c) half of the Arcan jig.

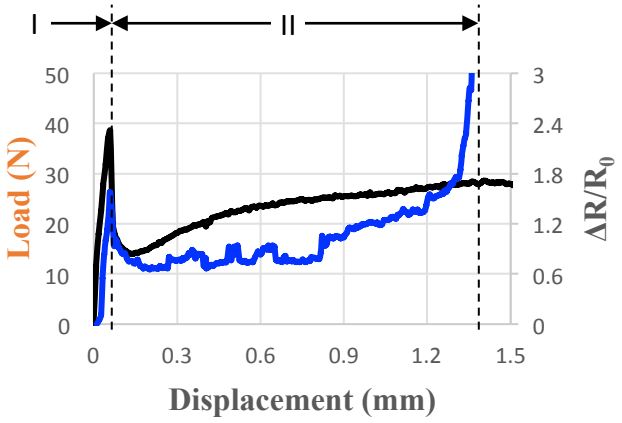


(a) (b)

Fig. 5. Tension results of three CFRP Z-pins; (a) stress and (b) fractional ER change.



(a)



(b)

Fig. 6. (a) full-range and (b) partially enlarged plots of Mode I results of single Z-pin reinforced CFRP laminate with debonding from one electrode; black lines indicate bridging forces; blue lines show fractional TTER changes; the red line in (a) indicates the bridging force given by a standard mechanical Z-pin for comparison.

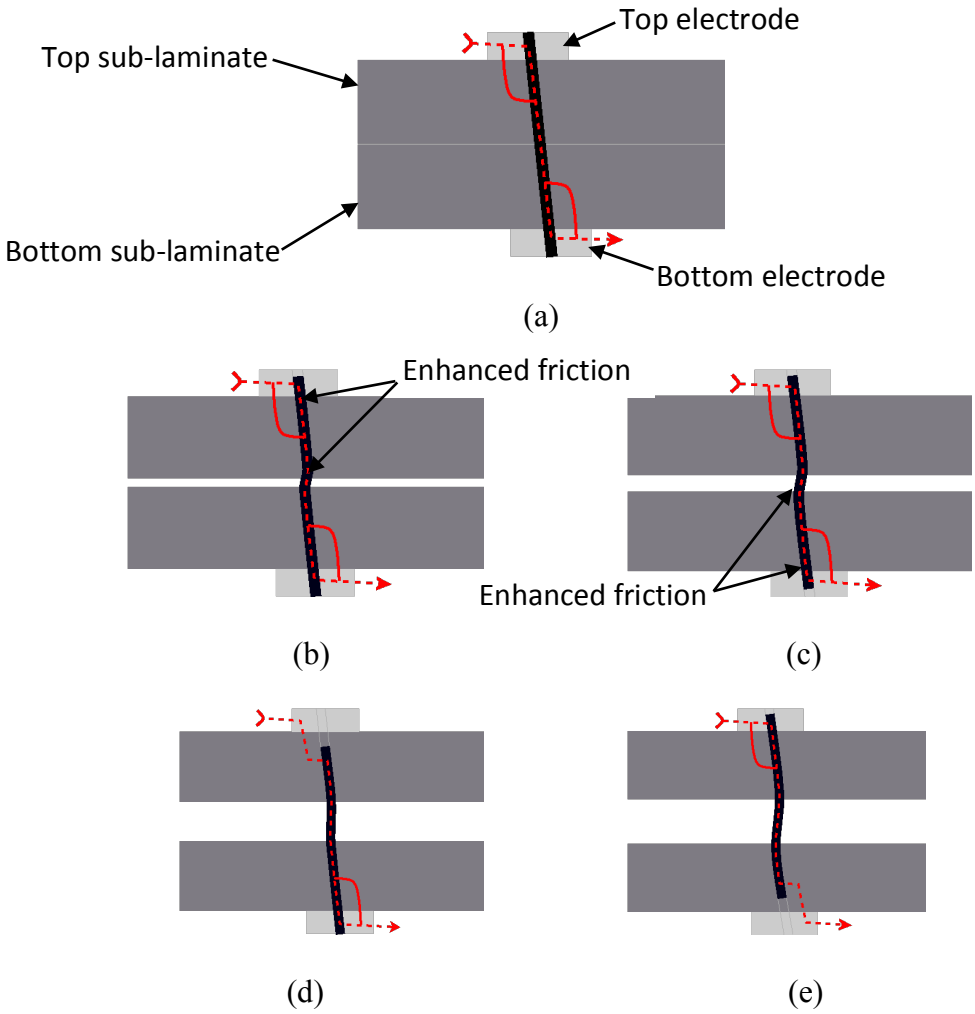


Fig. 7. Pull-out snapshots of the Z-pin with sensing configuration; (a) stage I: pre-debonding from electrode; stage II: pull-out from (b) top electrode and (c) bottom electrode; stage III: pull-out from (d) top sub-laminate and (e) bottom sub-laminate; dashed and solid red lines indicate current paths.

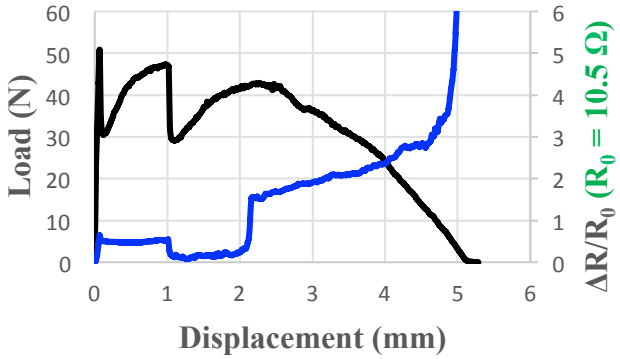


Fig. 8. Mode I results of CFRP laminate coupon with debonding from two electrodes; the black line indicates bridging force; the blue line shows the fractional TTER change.

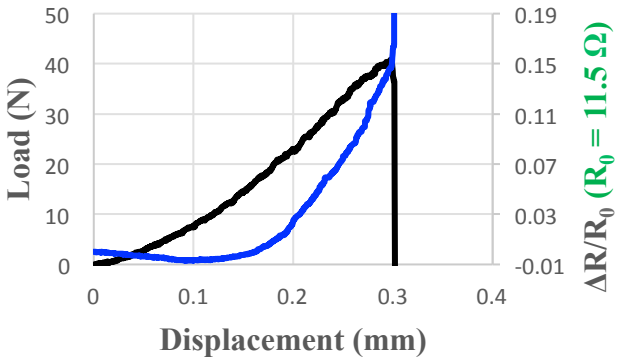
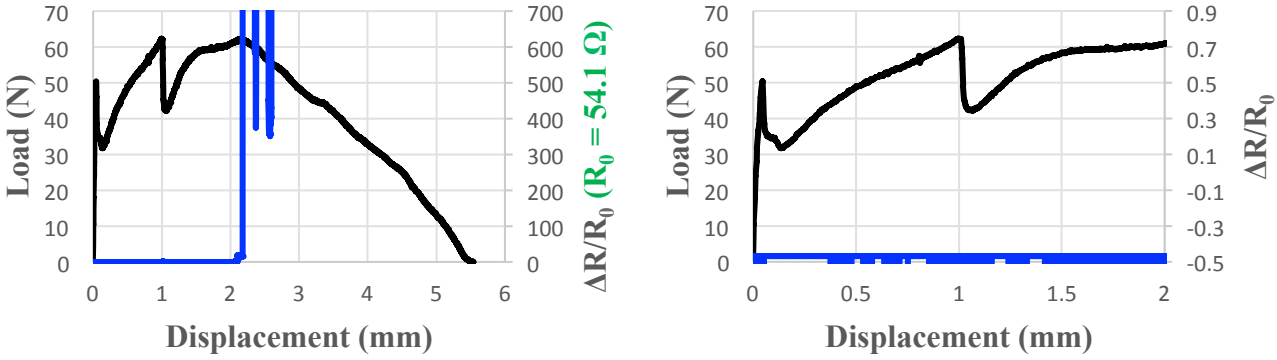


Fig. 9. Mode II results of single Z-pin reinforced CFRP laminate; the black line indicates bridging force; the blue line shows the fractional TTER change.



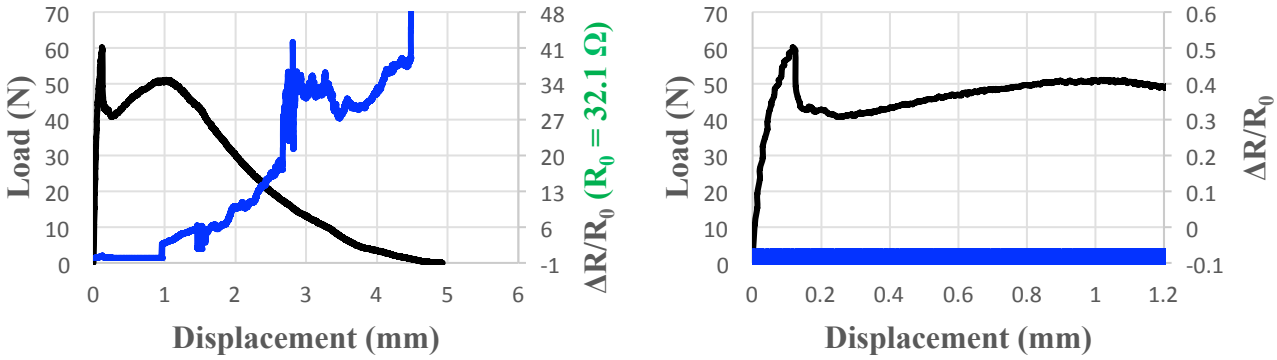


Fig. 10. Mode I results of single Z-pin reinforced GFRP laminates; (a) full-range and (b) partially enlarged plots of the coupon without sensing in stage III; (c) full-range and (d) partially enlarged plots of the coupon with sensing in stage III; black lines indicate bridging forces; blue lines show the fractional TTER changes.

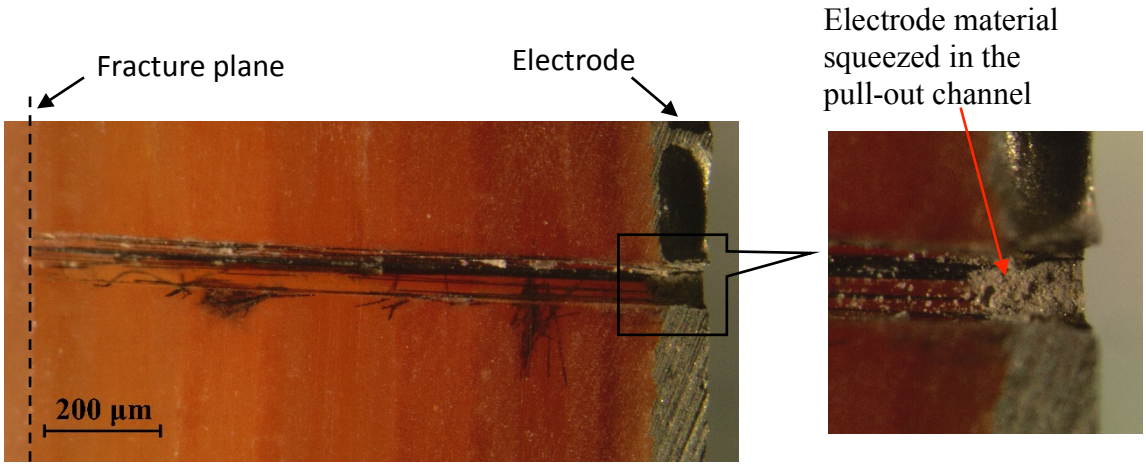


Fig. 11. Micrograph of the pull-out channel with residual Z-pin fibres.

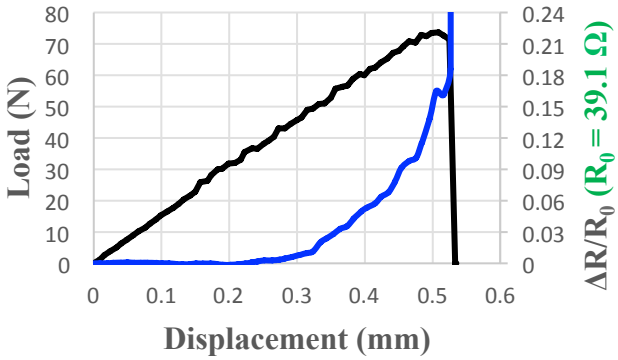


Fig. 12. Mode II results of single Z-pin reinforced GFRP laminate; the black line indicates bridging force; the blue line shows the fractional TTER change.